the QCP hypothesis also has consequences for the susceptibility amplitudes. Specifically, as $\omega \rightarrow 0$, $\chi''_P(\omega,T)/\omega$ should be controlled by a single variable representing the underlying magnetic length. In the upper right corner of Fig. 4, we plot χ''_P/ω as a function of such a variable, namely $\kappa(\omega = 0,T)$. The outcome is that $\chi''_P(\omega,T)/\omega$ is proportional to $\kappa(\omega = 0,T)^{\delta}$ where $\delta = (2 - \eta + Z)/Z = 3 \pm 0.3$, in agreement with theoretical expectations (*16*) for the critical exponents (η and z) associated with QCPs occurring in 2D insulating magnets.

To make the QCP hypothesis plausible, it would be useful to have evidence for an ordered state nearby in phase space. Because the high-T_c superconductors can be chemically tuned, what we are looking for are related compounds with magnetically ordered ground states. The most obvious is pure La_2CuO_4. However, in addition to the fact that the material itself seems far away in the phase space of Fig. 1A, the simple unit cell doubling that describes the antiferromagnetism of the material is remote from the long-period spin modulation that one would associate with the quartet of peaks seen in the magnetic response of $La_{1.86}Sr_{0.14}CuO_4$.

More interesting compounds are found when the phase space is expanded to consider ternary compounds, where elements other than or in addition to Sr^{2+} are substituted onto the La^{3+} site. When Nd^{3+} is substituted for La^{3+} while keeping the Sr^{2+} site occupancy (x) and hence hole density at 1/8, the material is no longer superconducting but exhibits instead a low-T phase characterized by magnetic Bragg peaks, corresponding to static magnetic order, at loci close to where the magnetic fluctuations are peaked in $La_{1.86}Sr_{0.14}CuO_4$. Although the full ternary phase diagram has not been searched, we have sketched what it might look like in Fig. 1, where the gray phase emerging close to the superconducting state is the ordered "striped phase," so named because one model describes it in terms of stripes of antiferromagnetic material separated by lines of charges (*17*).

More generally, experiments on the high-T_c materials can be thought of as travels through a 3D phase space such as that depicted in Fig. 1A, and the changes in behavior found on such travels can be associated with different features of the landscape coming into prominence depending on the height from which they are observed. At the higher $\hbar\omega$ and T values the (red) AFM phase, characterized by a very high coupling constant (~0.15 eV), is the most obvious feature. At the intermediate T values we probed, the dominant feature is the gray mountain where "striped" order has been found. Finally, at the lowest T, the superconducting instability dominates. The knowledge that the cuprates inhabit an interesting 3D phase space, together with our discovery that the spin fluctuations in one high-T_c material are as singular as the charge fluctuations, should simplify the task of understanding both the anomalous normal-state properties and the high-T_c superconductivity of the cuprates.

REFERENCES AND NOTES

1. B. Batlogg *et al*., *Electronic Properties of High-*T_c *Superconductors* (Springer, Berlin, 1993), p. 5.
2. F. Slakey *et al*., *Phys. Rev. B* **43**, 3764 (1991); Z. Schlesinger *et al*., *Phys. Rev. Lett.* **65**, 801 (1990).
3. T. R. Chien *et al*., *Phys. Rev. Lett.* **67**, 2088 (1991).
4. C. M. Varma *et al*., *ibid.* **63**, 1996 (1989).
5. B. Büchner *et al*., *ibid.* **73**, 1841 (1994).
6. J. M. Tranquada *et al*., *ibid.* **78**, 338 (1997); *Nature* **375**, 561 (1995).
7. D. Vaknin *et al*., *Phys. Rev. Lett.* **58**, 2802 (1987).
8. S. M. Hayden *et al*., *ibid.* **66**, 821 (1991); B. Keimer *et al*., *ibid.* **67**, 1930 (1991); B. Sternlieb *et al*., *Phys. Rev. B* **47**, 5320 (1993); J. Rossat-Mignod *et al*., *Physica B* **169**, 58 (1991).
9. S.-W. Cheong *et al*., *Phys. Rev. Lett.* **67**, 1791 (1991); T. E. Mason *et al*., *ibid.* **68**, 1414 (1992); T. R. Thurston *et al*., *Phys. Rev. B* **46**, 9128 (1992); M. Matsuda *et al*., *ibid.* **49**, 6958 (1994); K. Yamada *et al*., in preparation.
10. T. E. Mason *et al*., *Phys. Rev. Lett.* **71**, 919 (1993).
11. R. M. Moon *et al*., *Phys. Rev.* **181**, 883 (1969).
12. H. Sato and K. Maki, *Int. J. Magn.* **6**, 183 (1974); D. R. Noakes *et al*., *Phys. Rev. Lett.* **65**, 369 (1990).
13. We have used acoustic phonons in scans along $\mathbf{Q} = (2,\xi,0)$ and $(2,0,\nu)$ (orthorhombic notation) for $\hbar\omega = 2$ and 2.7 meV (sound velocity $\cong$ 23 meV − Å).
14. S. M. Hayden *et al*., *Phys. Rev. Lett.* **67**, 3622 (1991); D. C. Johnston, *J. Magn. Magn. Mater.* **100**, 218 (1991).
15. See overview by M. Continentino [*Phys. Rep.* **39**, 179 (1994)] and experiments by M. C. Aronson *et al*. [*Phys. Rev. Lett.* **75**, 725 (1995)], H. v. Löhneysen *et al*. [*ibid.* **72**, 3262 (1994)], D. Bitko *et al*., [*ibid.* **77**, 940 (1996)], and A. Husmann *et al*. [*Science* **274**, 1874 (1996)]. Earlier theoretical papers include those by M. Rasolt *et al*. [*Phys. Rev. Lett.* **53**, 798 (1984)] and S. Chakravarty *et al*. [*Phys. Rev. B* **39**, 2344 (1989)].
16. S. Sachdev and J. Ye, *Phys. Rev. Lett.* **69**, 2411 (1992); A. Chubukov *et al*., *Phys. Rev. B* **49**, 11919 (1994); A. J. Millis, *ibid.* **48**, 7183 (1993).
17. V. J. Emery and S. A. Kivelson, *Physica* **209**, 597 (1993); J. Zaanen and O. Gunnarsson, *Phys. Rev. B* **40**, 7391 (1989).

18. We thank B. Batlogg, S. Chakravarty, P. Littlewood, A. Millis, D. Pines, B. Statt, R. Walstedt, and especially S. Sachdev for helpful conversations; we thank K. N. Clausen, K. Bechgaard, and J. Kjems for hospitality at Risø; this work was supported by European Commission Large Installation Program, Engineering and Physical Sciences Research Council, North Atlantic Treaty Organization, Natural Sciences and Engineering Research Council, Canadian Institute for Advanced Research, and U.S. Department of Energy.

8 July 1997; accepted 26 September 1997

Direct Measurement of the Current-Phase Relation of a Superfluid ^{3}He-B Weak Link

S. Backhaus, S. V. Pereverzev,* A. Loshak, J. C. Davis, R. E. Packard

Direct measurements of the current-phase relation, I versus $\Delta\phi$, for a weak link coupling two reservoirs of B-phase superfluid helium-3 (^{3}He-B) were made over a wide range of temperatures. The weak link consists of a square array of 100-nanometer-diameter apertures. For temperatures T such that $T/T_c \geq 0.6$ (where T_c is the superfluid transition temperature), $I \propto \sin(\Delta\phi)$. At lower temperatures, $I(\Delta\phi)$ approaches a straight line. Several remarkable phenomena heretofore inaccessible to superconducting Josephson junctions, including direct observation of quantum oscillations and continuous knowledge of $\Delta\phi$, were also observed.

The general description of two coupled macroscopic quantum systems (such as superconductors, superfluids, or Bose-Einstein condensates) allows for the flow of supercurrents between the two.Theory has long predicted (*1*) that if the coupling is sufficiently weak, the mass current I depends on the phase difference between the two systems, $\Delta\phi$, as

$$I(\Delta\phi) = I_c \sin(\Delta\phi) \qquad (1)$$

where I_c is the critical current of the weak link. As the coupling becomes stronger, $I(\Delta\phi)$ should smoothly change to approach the strongly coupled case $I \propto \Delta\phi$.

For several decades, the only known systems described by Eq. 1 were superconductors, coupled either by tunnel junctions (the Josephson effect) or by metallic contacts whose spatial dimensions were comparable to the superconducting "healing length" ξ (Dayem bridges). This latter parameter is the characteristic length over which the wave function's amplitude is allowed to vary consistent with minimization of the energy of the system.

A microaperture in a thin wall should form the superfluid analog of a Dayem bridge (and thus act as a superfluid weak link) if the aperture diameter and wall thickness are near the superfluid healing length ξ. Researchers have long considered superfluid ^{3}He-B to be a good candidate to

Physics Department, University of California, Berkeley, CA 94720, USA.

*Permanent address: Institute for High Pressure Physics, Russian Academy of Sciences, Moscow, Russia.

display mass flow phenomena associated with Eq. 1 because it is a macroscopic quantum system, with healing length

$$\xi = \xi_0[1 - (T/T_c)]^{-1/2} \qquad (2)$$

where $T_c = 0.929$ mK, and $\xi_0 = 65$ nm at zero ambient pressure (*2*). Nevertheless, efforts in our laboratory (*3*) (using single apertures) and elsewhere (*4*) (using apertures and arrays of long thin tubes) did not show any evidence of weak coupling in superfluid ^{3}He.

In the late 1980s, a major advance was made in an experiment by Avenel, Varoquaux, and their co-workers, who studied flow of superfluid ^{3}He through a single microaperture in parallel with a much larger tube (*5*). The dynamics of the flow through the two openings were measured as a function of the driving force at two different frequencies. The observed dynamics were then recreated in a numerical simulation that required an assumed form of $I(\Delta\phi)$ as an input. The assumed $I(\Delta\phi)$ was similar to Eq. 1 but had adjustable parameters, namely I_c and a second parameter that controls the asymmetry of $I(\Delta\phi)$. A third adjustable parameter describes the relative inductances of the two flow paths. Values of the parameters were found that yielded good agreement between the observed and simulated responses near T_c (*5*). In particular, at temperatures above 0.8 T/T_c, the form of the best-fit $I(\Delta\phi)$ was close to a sine function, implying that near this temperature the aperture was nearly an ideal weak link. These results constituted the first evidence of ideal weak link behavior in superfluid ^{3}He. Magnetization transport experiments in superfluid ^{3}He have subsequently identified a method of creating quantum weak coupling of two spin reservoirs (*6*).

We have now developed a new type of ^{3}He weak link that consists of a square array of 4225 apertures, each 100 nm in diameter, separated by 3 μm, and positioned in a 50-nm-thick SiN window. The array was designed to behave like a single aperture with 4225 times the single-aperture current, therefore allowing a direct measurement of $I(\Delta\phi)$.

If this array connects two reservoirs of superfluid ^{3}He-B, an applied pressure head ΔP between the two reservoirs leads to mass-current oscillations (*7*) at frequency $f_Q = 2m_3\Delta P/\rho h$, where $2m_3$ is the mass of a Cooper pair, ρ is the liquid density, and h is the Planck constant. This phenomenon is consistent with a periodic $I(\Delta\phi)$ relation generically similar to Eq. 1, in combination with the phase evolution equation for macroscopic quantum systems:

$$\frac{d\Delta\phi}{dt} = -\frac{\Delta\mu}{\hbar} \qquad (3)$$

where t is time, $\hbar = h/2\pi$, and $\Delta\mu$ is the difference in chemical potential between two points, proportional to pressure head ($\Delta\mu = 2m_3\Delta P/\rho$). Both calculation and experiments have shown that the differential temperature term, which can appear in $\Delta\mu$, is negligible during this experiment.

To determine the $I(\Delta\phi)$ relation for this weak link, we used apparatus previously described (*7*). One sample of superfluid was confined within a disk-shaped region bounded by (i) a washer-shaped Kapton ring that had a soft membrane attached to its top side and (ii) a stiff membrane supporting a Si chip that contained the array on the lower side. This cell was similar to the type first used by Wirth and Zimmermann (*8*) and later developed by Avenel and Varoquaux (*9*). The cell was surrounded by superfluid (the second reservoir), which was in thermal contact with the heat exchanger of a refrigerator that could cool the liquid below 200 μK. The soft membrane was coated with a superconducting metal film and was adjacent to a metal actuator electrode and a superconducting quantum interference device (SQUID)–based displacement transducer that could detect motion of the membrane as small as 10^{-14} mHz$^{-1/2}$.

At some instant, we applied an electric potential step between the flexible membrane and the actuator to establish an initial pressure difference across the array. The displacement transducer detected the membrane's position $x(t)$ as it relaxed to its final equilibrium position x_f. Near the beginning of this transient, the pressure head was high enough that the quantum oscillations [arising from the combination of a 2π-periodic $I(\Delta\phi)$ and Eq. 3] were in the kilohertz range and could not easily be observed. However, as the pressure head relaxed (as a result of dissipation), the quantum oscillation frequency eventually dropped to a few tens of hertz, which allowed direct observation of the oscillations in the relaxation transient (Fig. 1). When the average pressure difference ΔP was not zero, the membrane oscillated at frequency $f_Q = 2m_3\Delta P/\rho h$.

When the average value of ΔP fell to zero and the average phase difference became constant, the dynamics of the coupled weak link–membrane system exhibited a different type of oscillation about the final equilibrium position. The frequency of these final oscillations was determined by the stiffness of the membrane and the kinetic inductance of the weak link. We refer to this situation as the pendulum mode of oscillation, because in this segment of the transient the equations of motion for $\Delta\phi$ can be cast into a form similar to that of a physical pendulum (*10*).

The real-time observation of both the quantum oscillations and the pendulum mode oscillations are remarkable features of this experiment because analogous phenomena have not been seen directly in the case of superconductors (there, the frequencies are normally in the gigahertz range). Our ability to detect these phenomena was due to at least two things: (i) The flow through all of the apertures indeed remained coherent, thus producing the 4225-fold amplification of the mass current compared with that in a single 100-nm-sized aperture, and (ii) the combination of Planck's constant, the liquid helium mass density, and the attainable pressure head

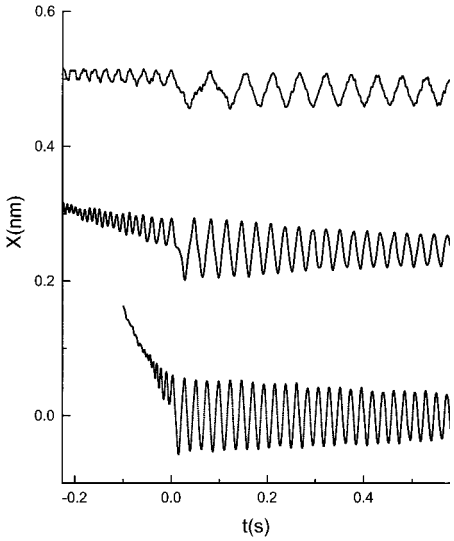

Fig. 1. Membrane displacement as a function of time at the end of the transient for temperatures 0.71 T/T_c (top), 0.56 T/T_c (center), and 0.41 T/T_c (bottom). The zero of time has been shifted so that the transition from the quantum oscillation to the pendulum mode occurs at $t = 0$ in all traces. The equilibrium position of each curve has been shifted vertically so that they do not overlap. When the average displacement x was not zero, the membrane oscillated at frequency $f_Q = 2m_3\Delta P/\rho h$, where $\Delta P = \alpha(x - x_f)$. After x reached x_f and the average phase became constant, the dynamics of the coupled weak link–membrane system exhibited the pendulum mode of oscillation. The frequency of this mode was determined by the stiffness of the membrane and the kinetic inductance of the weak link. In the few cycles after pendulum mode begins ($t = 0$), the most obvious evidence of the sine-like $I(\Delta\phi)$ can be seen in the raw data (at higher temperatures). The rate of change of position of the membrane, which is proportional to the current, fell to a low value as the membrane passed through the position at which $\Delta P = 0$. This is because at this point, the phase difference approaches π, where a sine-like current-phase relation would allow no current. At lower temperatures (for example, 0.41 T/T_c), this phenomenon disappeared as the $I(\Delta\phi)$ became linear in $\Delta\phi$. It was also absent in ^{4}He calibration tests.

range led to quantum oscillation at observable frequencies (below 100 Hz).

We directly determined the $I(\Delta\phi)$ relation by the following method. The displacement transducer output had been calibrated, so the recorded transient could be converted directly into a record of the soft membrane's position $x(t)$. The time derivative of $x(t)$, the known number of apertures N, and the membrane area A determined the instantaneous current through a single aperture

$$I(t) = \frac{\rho A}{N}\frac{dx}{dt} \quad (4)$$

The membrane's displacement from equilibrium was proportional to the instantaneous pressure head $\Delta P(t)$, that is, $\Delta P = \alpha(x - x_f)$. We directly determined the constant of proportionality α by measuring the linear dependence of the quantum oscillation frequency on the displacement of the membrane (*7*) [$f_Q = 2m_3\alpha(x - x_f)/\rho h$] near the beginning of the transient. At these higher pressures (≈10 mPa), the frequency could be extracted (in the kilohertz regime), although the actual details of $x(t)$ were obscured because the amplitude of membrane motion due to the quantum oscillations fell at least as $1/f_Q$ and because of noise from the wide-bandwidth nature of the measurement. The absolute knowledge of α gave the instantaneous phase difference by integrating Eq. 3

$$\Delta\phi(t) = \frac{-2m_3}{\rho\hbar}\int_0^t \alpha[x(t) - x_f]dt \quad (5)$$

This ability to directly and continuously determine $\Delta\phi$ based on Eq. 5 is a central feature of the experiment. By eliminating the common variable t from the known $I(t)$ and $\Delta\phi(t)$ we calculated $I(\Delta\phi)$.

The pendulum mode of the double-membrane cell involved out-of-phase motion of the membranes at frequencies ranging from 5 to 55 Hz. However, there was another normal mode where the two membranes moved in phase at much higher frequencies. Before applying Eqs. 4 and 5, we filtered the data with a low-pass filter (24 dB per octave) using cutoff frequencies varying from 60 to 160 Hz. Above this frequency, the normal mode associated with the in-phase motion of both diaphragms introduced complications to the analysis.

The function $I(\Delta\phi)$ could have been determined from either of the two distinct parts of the transient. We could have used the quantum oscillations themselves for the analysis if the relaxation transient was slow enough so that the bandwidth in the filtered data was sufficient to capture several higher harmonics of the oscillation frequency. Alternatively, we could have analyzed the motion in the pendulum-mode regime, which had a lower frequency (5 to 55 Hz) than the quantum oscillation.

We performed the above analysis on both segments of the transient, and in the regime where both methods were suitable, we obtained identical results for $I(\Delta\phi)$. For consistency, we present only the results from the pendulum oscillations because the analysis from this motion can span our entire accessible temperature range.

We chose the zero of time to correspond to the end of the quantum oscillation period and the beginning of the pendulum motion. To enhance the signal-to-noise ratio, we continued the integration forward in time through two to three oscillations. The measured $I(\Delta\phi)$ was periodic in $\Delta\phi$ with period 2π. We effectively signal averaged $I(\Delta\phi)$ by translating the data from the regions 2π to 4π and 4π to 6π onto the first interval, 0 to 2π, and averaging these curves together. We then took the results from multiple transients (typically 10 to 50) at a given temperature and averaged all of the values of I corresponding to a given $\Delta\phi$.

Figure 2 shows part of the results of this analysis, the shape of the functions $I(\Delta\phi)$ for several temperatures between 0.28 T/T_c and 0.85 T/T_c. At higher temperatures, $I(\Delta\phi)$ was nearly a sine function, indicating that the aperture array was a perfect weak link. As T dropped and the healing length shortened (Eq. 2), $I(\Delta\phi)$ began to depart from the sine function and became noticeably less curved near $\Delta\phi = \pm\pi/2$. This behavior is expected theoretically: The $I(\Delta\phi)$ relation evolves from sine-like to almost linear in $\Delta\phi$. Our results confirm the deductions of (*5*) by a direct method, and they provide new information about the specific form of $I(\Delta\phi)$ over a wide range in temperature.

The results presented here serve as an experimental test for theoretical models of weak links in ^{3}He-B. We cannot compare our results directly with a single theory because no single model adequately covers the entire geometry, boundary conditions, and T range represented in this experiment. Several authors have computed $I(\Delta\phi)$ for various aperture parameters (*10*–*15*), but space does not permit comparison with all of these predictions. However, in brief, the results for a pinhole-like aperture (*12*) (that is, diameter $\ll\xi$, an aperture that does not distort the order parameter) fit the shape of the $I(\Delta\phi)$ data well at the higher temperatures, and the predictions for a finite-size aperture (*15*) fit the shape at the lower temperatures. This correspondence is the theoretically expected trend (Fig. 2) because at higher temperatures the healing length is considerably greater than our aperture diameter, whereas the converse is true at the lower temperatures.

The critical current I_c of the weak link can be defined as the maximum observed current in the function $I(\Delta\phi)$. The data reported here are from a single cooldown below T_c (to avoid the variations in the

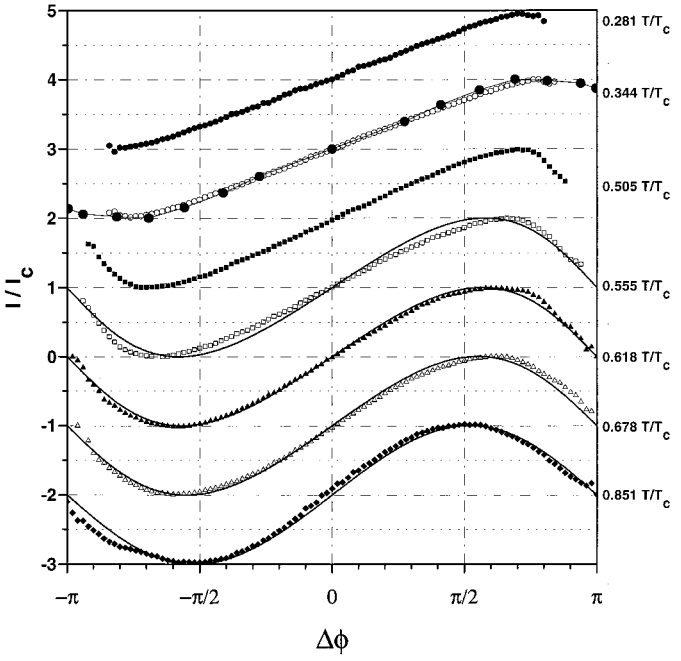

Fig. 2. Shape of the function $I(\Delta\phi)$, as calculated from the data, for seven temperatures in the range from 0.28 T/T_c to 0.85 T/T_c. The complete form of $I(\Delta\phi)$ was first calculated, and then the whole curve was divided by the maximum current at the same temperature to yield the normalized shape of $I(\Delta\phi)$. Each curve is shifted vertically along the normalized current axis by one unit for clarity of presentation. At higher temperatures, $I(\Delta\phi)$ is a sine function, indicating that the aperture array behaved as a perfect weak link. At lower temperatures, $I(\Delta\phi)$ departs from the sine function. The phase at which I_{max} is achieved becomes steadily greater than $\Delta\phi = \pi/2$ with falling temperatures until $I(\Delta\phi)$ approaches a straight line. For temperatures 0.555 T/T_c through 0.851 T/T_c, the shape of the predicted $I(\Delta\phi)$ for a pinhole (*12*) is plotted (as a solid line) along with the data for comparison. For 0.344 T/T_c, the predicted shape of $I(\Delta\phi)$ for an aperture of similar dimensions near this temperature (*15*) is plotted (solid circles) along with the data.

magnitude of I_c that have been observed between cooldowns). We checked the repeatability of these data as a function of T by sweeping temperature down and up and checking that the observations remained the same. The most striking aspect of the I_c data is that, for $1 - (T/T_c) > 0.3$, the values were several times greater than the maximum depairing (*16*) currents in bulk ^{3}He-B (Fig. 3). Several calculations predict such enhancement (*11*, *12*, *14*). The observed quadratic growth in I_c is a feature predicted (*17*) for diffuse-scattering boundary conditions for quasiparticles. We also note that I_c seemed to fall to zero well below T_c of the bulk liquid.

The techniques and measurements reported here create several opportunities for macroscopic quantum physics research in superfluid ^{3}He. Continuous measurements of $\Delta\phi$ (using the absolute pressure calibration from the Josephson frequency relation) as demonstrated here can be used in experiments focusing on macroscopic quantum phase. Further, the detailed information on the $I(\Delta\phi)$ of a superfluid ^{3}He weak link will allow the future development of a superfluid "two-slit" interferometer. This device, which is analogous to the superconducting dc-SQUID and is sometimes called a "superfluid quantum interference gyroscope," should be a sensitive rotation sensor (*18*).

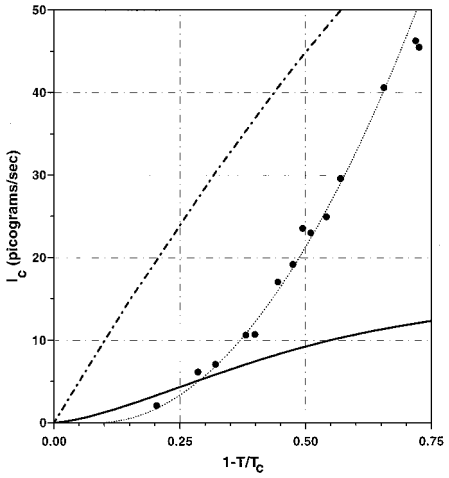

Fig. 3. The measured values of the critical current for the microaperture array weak link divided by 4225 (circles) as a function of $1 - (T/T_c)$. Here we have used the I_c that is derived from analysis of the pendulum mode; the values are consistent with those derived from the quantum oscillations. For $1 - (T/T_c) > 0.3$, the values of I_c are several times greater than the maximum depairing currents in bulk ^{3}He-B (solid line) (*16*). The predictions for a pinhole aperture (*12*) (dot-dash line) are shown for comparison. The data are best fit by $I_c = 104[1 - (T/T_{ca})]^2$ pg/s, where $T_{ca} = 0.85$ mK (dotted line). The observed quadratic growth in I_c is a feature predicted to be associated with diffuse-scattering boundary conditions for the ^{3}He quasiparticles (*17*).

REFERENCES AND NOTES

1. B. D. Josephson, thesis, Trinity College, Cambridge University (1962); P. W. Anderson, in *Lectures on the Many-Body Problem*, E. R. Caianello, Ed. (Academic Press, New York, 1964), p. 113–135; R. P. Feynman, *The Feynman Lectures on Physics* (Addison-Wesley, New York, 1965), sect. 21-9.
2. In contrast, the superfluid ^{4}He healing length is ≈0.1 nm. Because apertures of this diameter are not presently available, it is quite challenging to search for these phenomena in superfluid ^{4}He.
3. J. Steinhauer, thesis, University of California, Berkeley (1995).
4. B. C. Crooker, thesis, Cornell University, Ithaca, NY (1984); M. T. Manninen and J. P. Pekola, *Phys. Rev. Lett.* **48**, 812, (1982).
5. O. Avenel and E. Varoquaux, *Jpn. J. Appl. Phys.* **26**, 26 (1987); *Phys. Rev. Lett.* **60**, 416 (1988); E. Varoquaux, O. Avenel, G. Ihas, R. Salmelin, *Physica B* **178**, 309 (1990).
6. A. S. Borovik-Romanov *et al.*, *JETP Lett.* **47**, 478 (1988).
7. S. V. Pereverzev, A. Loshak, S. Backhaus, J. C. Davis, R. E. Packard, *Nature* **388**, 449 (1997).
8. F. H. Wirth and W. Zimmermann Jr., *Physica B* **107**, 579 (1981).
9. O. Avenel and E. Varoquaux, in *Proceedings of the 10th International Cryogenic Engineering Conference*, G. Klipping and I. Klipping, Eds. (Butterworths, Guilford, 1986), pp. 587–589.
10. H. Monien and L. Tewordt, *J. Low Temp. Phys.* **62**, 277 (1986).
11. J. R. Hook, *Jpn. J. Appl. Phys.* **26**, 159 (1987).
12. J. Kurkijärvi, *Phys. Rev. B* **38**, 11184 (1988).
13. E. V. Thuneberg, *Europhys. Lett.* **7**, 441 (1988).
14. S. Ullah and A. Fetter, *Phys. Rev. B* **39**, 4186 (1989).
15. E. V. Thuneberg, J. Kurkijärvi, J. A. Sauls. *Physica B* **165/166**, 755 (1990).
16. K. W. Jacobsen and H. Smith, *J. Low Temp. Phys.* **67,** 83 (1987).
17. N. B. Kopnin, *JETP Lett.* **43,** 701 (1986).
18. R. E. Packard and S. Vitale, *Phys. Rev. B* **46**, 3540 (1992).

19. Earlier versions of this project were aided by J. Steinhauer, K. Schwab, and Yu. Mukharsky. E. W. Hudson contributed to the data acquisition system and D. Duarte and K. Shokhirev helped with the analysis of data. We thank S. Vitale, R. Y. Chiao, and L. Bildsten for valuable discussions. The aperture array was constructed in the Berkeley Microfabrication Laboratory. The research was supported in part by grants from the National Science Foundation, the Office of Naval Research, and the David and Lucile Packard Foundation.

6 August 1997; accepted 7 October 1997

A Tribosphenic Mammal from the Mesozoic of Australia

Thomas H. Rich, Patricia Vickers-Rich, Andrew Constantine, Timothy F. Flannery, Lesley Kool, Nicholas van Klaveren

A small, well-preserved dentary of a tribosphenic mammal with the most posterior premolar and all three molars in place has been found in Aptian (Early Cretaceous) rocks of southeastern Australia. In most respects, dental and mandibular anatomy of the specimen is similar to that of primitive placental mammals. With the possible exception of a single tooth reported as Eocene in age, terrestrial placentals are otherwise unknown in Australia until the Pliocene. This possible Australian placental is similar in age to *Prokennalestes* from the late Aptian/early Albian Khoboor Beds of Mongolia, the oldest currently accepted member of the infraclass Placentalia.

The known Cretaceous fossil record of placental mammals comes primarily from three areas: Mongolia, Middle Asia (Uzbekistan, Kazakhstan, and Tajikistan), and the Western Interior of North America. In addition, single genera have been described from India and Baja, California, and single teeth have been reported from France and Mississippi (Fig. 1). Except for the Mongolian *Prokennalestes* and Uzbekistani *Bobolestes*, all are Late Cretaceous in age. This record, based on about 2 dozen genera, is meager compared with that of Cenozoic placentals. In a roughly comparable time span, there are literally thousands of Cenozoic placental genera known.

T. H. Rich, Museum of Victoria, Post Office Box 666E, Melbourne, Victoria 3001, Australia.
P. Vickers-Rich, A. Constantine, L. Kool, N. van Klaveren, Earth Sciences Department, Monash University, Clayton, Victoria 3001, Australia.
T. F. Flannery, Australian Museum, 6 College Avenue, Sydney South, New South Wales 2000, Australia.

Because Mesozoic tribosphenic mammals were unknown on all Southern Hemisphere continents in 1986, in that year Jóse Bonaparte proposed that subsequent to the end of the Jurassic, the Gondwanan mammalian fauna had evolved completed isolated from faunas on the northern continents until the end of the Cretaceous or the beginning of the Paleocene (*1*). According to Bonaparte, during this period of isolation, marsupials and placentals arose from more primitive tribosphenic or near tribosphenic mammals in Laurasia. According to this hypothesis, tribosphenic mammals of any kind reached South America for the first time near the Cretaceous-Tertiary boundary, from North America. From South America, marsupials then dispersed across Antarctica to Australia.

The concept of the complete isolation of the Gondwana continents from tribosphenic mammals until the end of the Cretaceous was first challenged with the an-